

# Optimal Trajectory Planning for Cinematography with Multiple Unmanned Aerial Vehicles

Alfonso Alcantara<sup>a</sup>, Jesus Capitan<sup>a</sup>, Rita Cunha<sup>b</sup>, Anibal Ollero<sup>a</sup>

<sup>a</sup>GRVC Robotics Laboratory, University of Seville, Spain.

<sup>b</sup>Institute for Systems and Robotics, Instituto Superior Tcnico, Universidade de Lisboa, Portugal.

## Abstract

This paper presents a method for planning optimal trajectories with a team of *Unmanned Aerial Vehicles* (UAVs) performing autonomous cinematography. The method is able to plan trajectories online and in a distributed manner, providing coordination between the UAVs. We propose a novel non-linear formulation for this challenging problem of computing multi-UAV optimal trajectories for cinematography; integrating UAVs dynamics and collision avoidance constraints, together with cinematographic aspects like smoothness, gimbal mechanical limits and mutual camera visibility. We integrate our method within a hardware and software architecture for UAV cinematography that was previously developed within the framework of the *MultiDrone* project; and demonstrate its use with different types of shots filming a moving target outdoors. We provide extensive experimental results both in simulation and field experiments. We analyze the performance of the method and prove that it is able to compute online smooth trajectories, reducing jerky movements and complying with cinematography constraints.

**Keywords:** Optimal trajectory planning, UAV cinematography, Multi-UAV coordination

## 1. Introduction

Drones or *Unmanned Aerial Vehicles* (UAVs) are spreading fast for aerial photography and cinematography, mainly due to their maneuverability and their capacity to access complex filming locations in outdoor settings. From the application point of view, UAVs present a remarkable potential to produce unique aerial shots at reduced costs, in contrast with other alternatives like dollies or static cameras. Additionally, the use of teams with multiple UAVs opens even more the possibilities for cinematography. On the one hand, large-scale events can be addressed by filming multiple action points concurrently or sequentially. On the other hand, the combination of shots with multiple views or different camera motions broadens the artistic alternatives for the *director*.

Currently, most UAVs in cinematography are operated in manual mode by an expert pilot. Besides, an additional qualified operator is required to control the camera during the flight, as taking aerial shots can be a complex and overloading task. Even so, the manual operation of UAVs for aerial cinematography is still challenging, as multiple aspects need to be considered: performing smooth trajectories to achieve aesthetic videos, tracking actors to be filmed, avoiding collisions with

potential obstacles, keeping other cameras out of the field of view, etc.

There exist commercial products (e.g., *DJI Mavic* [1] or *Skydio* [2]) that cope with some of the aforementioned complexities implementing semi-autonomous functionalities, like *auto-follow* features to track an actor or simplistic collision avoidance. However, they do not address cinematographic principles for multi-UAV teams, as e.g., planning trajectories considering gimbal physical limitations or inter-UAV visibility. Therefore, solutions for autonomous filming with multiple UAVs are of interest. Some authors [3] have shown that planning trajectories ahead several seconds is required in order to fulfill with cinematographic constraints smoothly. Others [4, 5] have even explored the multi-UAV problem, but online trajectory planning for multi-UAV cinematography outdoors is still an open issue.

In this paper, we propose a method for online planning and execution of trajectories with a team of UAVs taking cinematography shots. We develop an optimization-based technique that runs on the UAVs in a distributed fashion, taking care of the control of the UAV and the gimbal motion simultaneously. Our method aims at providing smooth trajectories for visually pleasant video output; integrating cinematographic constraints imposed by the shot types, the gimbal physical limits, the mutual visibility between cameras and the avoidance of collisions.

This work has been developed within the framework of the EU-funded project *MultiDrone*<sup>1</sup>, whose objective was to create a complete system for autonomous cinematography with multi-

<sup>\*</sup>This work was partially funded by the European Union's Horizon 2020 research and innovation programme under grant agreements No 731667 (MultiDrone), and by the MULTICOP project (Junta de Andalucia, FEDER Programme, US-1265072).

Email addresses: aamarin@us.es (Alfonso Alcantara), jcapitan@us.es (Jesus Capitan), rita@isr.utl.pt (Rita Cunha), aollero@us.es (Anibal Ollero)

<sup>1</sup><https://multidrone.eu>.



Figure 1: Cinematography application with two UAVs filming a cycling event. Bottom, aerial view of the experiment with two moving cyclists. Top, images taken from the cameras on board each UAV.

ples UAVs in outdoor sport events (see Figure 1). MultiDrone addressed different aspects to build a complete architecture: a set of high-level tools so that the cinematography director can define shots for the mission [6]; planning methods to assign and schedule the shots among the UAVs efficiently and considering battery constraints [7]; vision-based algorithms for target tracking on the camera image [8], etc. In this paper, we focus on the autonomous execution of shots with a multi-UAV team. We assume that the director has designed a mission with several shots; and that there is a planning module that has assigned a specific shot to each UAV. Then, our objective is to plan trajectories in order to execute all shots online in a coordinated manner.

### 1.1. Related work

Optimal trajectory planning for UAVs is a commonplace problem in the robotics community. A typical approach is to use optimization-based techniques to generate trajectories from polynomial curves minimizing their derivative terms for smoothness, e.g., the fourth derivative or snap [9, 10]. This polynomial trajectories have also been applied to optimization problems with multiple UAVs [11]. *Model Predictive Control* (MPC) is another widespread technique for optimal trajectory planning [12], a dynamic model of the UAV is used for predicting and optimizing trajectories ahead within a receding horizon. Some authors [13] have also used MPC-based approaches for multi-UAV trajectory planning with collision avoidance and non-linear models. In the context of multi-UAV target tracking, others [14, 15] have combined MPC with potential fields to address the non-convexity induced by collision avoidance constraints. In [16], a constrained optimization problem is formulated to maintain a formation where a leader UAV takes pictures for inspection in dark spaces, while others illuminate the target spot supporting the task. The system is used for aerial documentation within historical buildings.

Additionally, there are works in the literature just for target tracking with UAVs, proposing alternative control techniques

like classic PID [17] or LQR [18] controllers. The main issues with all these methods for trajectory planning and target tracking are that they either do not consider cinematographic aspects explicitly or do not plan ahead in time for horizons long enough.

In the computer animation community, there are several works related with trajectory planning for the motion of virtual cameras [19]. They typically use offline optimization to generate smooth trajectories that are visually pleasant and comply with certain cinematographic aspects, like the *rule of thirds*. However, many of them do not ensure physical feasibility to comply with UAV dynamic constraints and they assume full knowledge of the environment map. In terms of optimization functions, several works consider similar terms to achieve smoothness. For instance, authors in [20] model trajectories as polynomial curves whose coefficients are computed to minimize snap (fourth derivative). They also check dynamic feasibility along the planned trajectories, and the user is allowed to adjust the UAV velocity at execution time. A similar application to design UAV trajectories for outdoor filming is proposed in [21]. Timed reference trajectories are generated from 3D positions specified by the user, and the final timing of the shots is addressed designing easing curves that drive the UAV along the planned trajectory (i.e., curves that modify the UAV velocity profile). In [22], aesthetically pleasant footage is achieved by penalizing the snap of the UAV trajectory and the jerk (third derivative) of the camera motion. An iterative quadratic optimization problem is formulated to compute trajectories for the camera and the look-at point (i.e., the place where the camera is pointing at). They also include collision avoidance constraints, but the method is only tested indoors.

Although these articles on computer graphics approach the problem mainly through offline optimization, some of them have proposed options to achieve real-time performance, like planning in a *toric space* [23] or interpolating polynomial curves [24, 21]. In general, these works present interesting theoretical properties, but they are restricted to offline optimization with a fully known map of the scenario and static or close-to-static guided tour scenes, i.e., without moving actors.

In the robotics literature, there are works focusing more on filming dynamic scenes and complying with physical UAV constraints. For example, authors in [25] propose to detect limbs movement of a human for outdoor filming. Trajectory planning is performed online with polynomial curves that minimize snap. In [26, 3], they present an integrated system for outdoor cinematography, combining vision-based target localization with trajectory planning and collision avoidance. For optimal trajectory planning, they apply gradient descent with differentiable cost functions. Smoothness is achieved minimizing trajectory jerk; and shot quality by defining objective curves fulfilling cinematographic constraints associated with relative angles w.r.t. the actor and shot scale. Cinematography optimal trajectories have also been computed in real time through receding horizon with non-linear constraints [27]. The user inputs framing objectives for one or several targets on the image, and errors of the image target projections, sizes and relative viewing angles are minimized; satisfying collision avoidance constraints and target visibility. The method behaves well for online numerical

References	Online	Scene	UAVs Dynamics	Collision Avoidance	Mutual Visibility	Outdoors	Multiples UAVs
[23]	✗	Static	✗	✗	✗	✗	✗
[20]	✗	Static	✓	✗	✗	✓	✗
[22]	✗	Static	✓	✓	✗	✗	✗
[21]	✗	Static	✓	Actor	✗	✓	✗
[24]	✗	Dynamic	✗	✗	✗	✗	✗
[27]	✓	Dynamic	✓	✓	✓	✗	✗
[4]	✓	Dynamic	✓	Actor	✓	✗	✓
[25]	✓	Dynamic	✓	Actor	✗	✓	✗
[5]	✓	Dynamic	✓	✓	✓	✗	✓
[26]	✓	Dynamic	✓	✓	✓	✓	✗
[3]	✓	Dynamic	✓	✓	✓	✓	✗
Ours	✓	Dynamic	✓	✓	✓	✓	✓

Figure 2: Related works on trajectory planning for UAV cinematography. We indicate whether computation is online or not, the type of scene and constraints they consider, and their capacity to handle outdoor applications and multiples UAVs.

optimization, but it is only tested in indoor settings.

Some of the aforementioned authors from robotics have also approached UAV cinematography applying machine learning techniques. In particular, learning from demonstration to imitate professional cameraman’s behaviors [28] or reinforcement learning to achieve visually pleasant shots [29]. In general, most of these cited works on robotics present results quite interesting in terms of operation outdoors or online trajectory planning, but they always restrict to a single UAV.

Regarding methods for multiple UAVs, there is some related work which is worth mentioning. In [4], a non-linear optimization problem is solved in a receding horizon fashion, taking into account collision avoidance constraints with the filmed actors and between the UAVs. Aesthetic objectives are introduced by the user as virtual reference trails. Then, UAVs receive current plans from all others at each planning iteration and compute collision-free trajectories sequentially. A UAV toric space is proposed in [5] to ensure that cinematographic properties and dynamic constraints are ensured along the trajectories. Non-linear optimization is applied to generate polynomial curves with minimum curvature variation, accounting for target visibility and collision avoidance. The motion of multiple UAVs around dynamic targets is coordinated by means of a centralized master-slave approach to solve conflicts. Even though these works present promising results for multi-UAV teams, they are only demonstrated at indoor scenarios where a *Vicon* motion capture system provides accurate positioning for all targets and UAVs.

To sum up, Figure 2 shows a table with the main related works on trajectory planning for UAV cinematography and their corresponding properties.

## 1.2. Contributions

We propose a novel method to plan online optimal trajectories for a set of UAVs executing cinematography shots. The optimization is performed in a distributed manner, and it aims for smooth trajectories complying with dynamic and cinematographic constraints. We extend our previous work [30] in optimal trajectory planning for UAV cinematography as follows:

(i) we cope with multiple UAVs integrating new constraints for inter-UAV collisions and mutual visibility; (ii) we present additional simulation results to evaluate the method with different types of shots; and (iii) we demonstrate the system in field experiments with multiple UAVs filming dynamic scenes. In particular, our main contributions are the following:

- We propose a novel formulation of the trajectory planning problem for UAV cinematography. We model both UAV and gimbal motion (Section 2), but decouple their control actions.
- We propose a non-linear, optimization-based method for trajectory planning (Section 3). Using a receding horizon scheme, trajectories are planned and executed in a distributed manner by a team of UAVs providing multiple views of the same scene. The method considers UAV dynamic constraints, and imposes them to avoid predefined no-fly zones or collisions with others. Cinematographic aspects imposed by shot definition, camera mutual visibility and gimbal physical bounds are also addressed. Trajectories smoothing UAV and gimbal motion are generated to achieve aesthetic video footage.
- We describe the complete system architecture on board each UAV and the different types of shot considered (Section 4). The architecture integrates target tracking with trajectory planning and it is such that different UAVs can be executing different types of shot simultaneously.
- We present extensive experimental results (Section 5) to evaluate the performance of our method for different types of shot. We prove that our method is able to compute smooth trajectories reducing jerky movements in real time, and complying with the cinematographic restrictions. Then, we demonstrate our system in field experiments with three UAVs planning trajectories online to film a moving actor (Section 6).

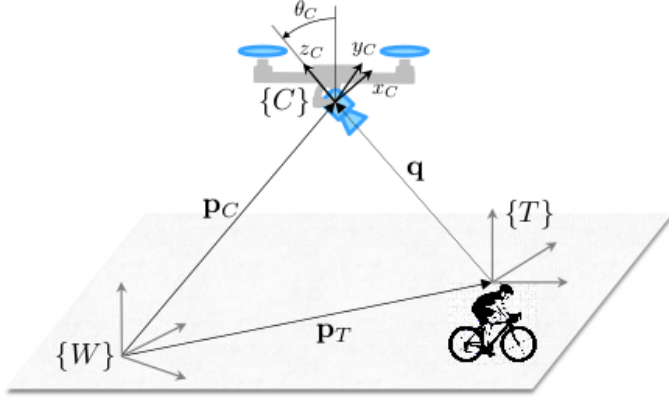


Figure 3: Definition of reference frames used. The origins of the camera and quadrotor frames coincide. The camera points to the target.

## 2. Dynamic Models

This section presents our dynamic models for UAV cinematographers. We model the UAV as a quadrotor with a camera mounted on a gimbal of two degrees of freedom.

### 2.1. UAV model

Let  $\{W\}$  denote the world reference frame with origin fixed in the environment and East-North-Up (ENU) orientation. Consider also three additional reference frames (see Figure 3): the quadrotor reference frame  $\{Q\}$  attached to the UAV with origin at the center of mass, the camera reference frame  $\{C\}$  with  $z$ -axis aligned with the optical axis but with opposite sign, and the target reference frame  $\{T\}$  attached to the moving target that is being filmed. For simplicity, we assumed that the origins of  $\{Q\}$  and  $\{C\}$  coincide.

The configuration of  $\{Q\}$  with respect to  $\{W\}$  is denoted by  $(\mathbf{p}_Q, R_Q) \in \mathbb{SE}(3)$ , where  $\mathbf{p}_Q \in \mathbb{R}^3$  is the position of the origin of  $\{Q\}$  expressed in  $\{W\}$  and  $R_Q \in \mathbb{SO}(3)$  is the rotation matrix from  $\{Q\}$  to  $\{W\}$ . Similarly, the configurations of  $\{T\}$  and  $\{C\}$  with respect to  $\{W\}$  are denoted by  $(\mathbf{p}_T, R_T) \in \mathbb{SE}(3)$  and  $(\mathbf{p}_C, R_C) \in \mathbb{SE}(3)$ , respectively.

We model the quadrotor dynamics as a linear double integrator model:

$$\begin{aligned} \dot{\mathbf{p}}_Q &= \mathbf{v}_Q \\ \dot{\mathbf{v}}_Q &= \mathbf{a}_Q, \end{aligned} \quad (1)$$

where  $\mathbf{v}_Q = [v_x \ v_y \ v_z]^T \in \mathbb{R}^3$  is the linear velocity and  $\mathbf{a}_Q = [a_x \ a_y \ a_z]^T \in \mathbb{R}^3$  is the linear acceleration. We assume that the linear acceleration  $\mathbf{a}_Q$  takes the form:

$$\mathbf{a}_Q = -g\mathbf{e}_3 + R_Q \frac{T}{m} \mathbf{e}_3, \quad (2)$$

where  $m$  is the quadrotor mass,  $g$  the gravitational acceleration,  $T \in \mathbb{R}$  the scalar thrust, and  $\mathbf{e}_3 = [0 \ 0 \ 1]^T$ .

For the sake of simplicity, we use the 3D acceleration  $\mathbf{a}_Q$  as control input; although the thrust  $T$  and rotation matrix  $R_Q$  could also be recovered from 3D velocities and accelerations.

If we restrict the yaw angle  $\psi_Q$  to keep the quadrotor's front pointing forward in the direction of motion such that:

$$\psi_Q = \text{atan2}(v_y, v_x), \quad (3)$$

then the thrust  $T$  and the Z-Y-X Euler angles  $\lambda_Q = [\phi_Q, \theta_Q, \psi_Q]^T$  can be obtained from  $\mathbf{v}_Q$  and  $\mathbf{a}_Q$  according to:

$$\begin{cases} T = m\|\mathbf{a}_Q + g\mathbf{e}_3\| \\ \psi_Q = \text{atan2}(v_y, v_x) \\ \phi_Q = -\arcsin((a_y \cos(\psi_Q) - a_x \sin(\psi_Q))/\|\mathbf{a}_Q + g\mathbf{e}_3\|) \\ \theta_Q = \text{atan2}(a_x \cos(\psi_Q) + a_y \sin(\psi_Q), a_z + g) \end{cases} \quad (4)$$

### 2.2. Gimbal angles

Let  $\lambda_C = [\phi_C, \theta_C, \psi_C]^T$  denote the Z-Y-X Euler angles that parametrize the rotation matrix  $R_C$ , such that:

$$R_C = R_z(\psi_C)R_y(\theta_C)R_x(\phi_C). \quad (5)$$

In our system, we decouple gimbal motion with an independent gimbal attitude controller that ensures that the camera is always pointing towards the target during the shot, as in [3]. This reduces the complexity of the planning problem and allows us to control the camera based on local perception feedback if available, accumulating less errors. We also consider that the time-scale separation between the "faster" gimbal dynamics and "slower" quadrotor dynamics is sufficiently large to neglect the gimbal dynamics and assume an exact match between the desired and actual orientations of the gimbal. In order to define  $R_C$ , let us introduce the relative position:

$$\mathbf{q} = [q_x \ q_y \ q_z]^T = \mathbf{p}_C - \mathbf{p}_T, \quad (6)$$

and assume that the UAV is always above the target, i.e.,  $q_z > 0$ , and not directly above the target, i.e.,  $[q_x \ q_y] \neq 0$ . Then, the gimbal orientation  $R_C$  that guarantees that the camera is aligned with the horizontal plane and pointing towards the target is given by:

$$\begin{aligned} R_C &= \begin{bmatrix} -\frac{\mathbf{q} \times \mathbf{q} \times \mathbf{e}_3}{\|\mathbf{q} \times \mathbf{q} \times \mathbf{e}_3\|} & \frac{\mathbf{q} \times \mathbf{e}_3}{\|\mathbf{q} \times \mathbf{e}_3\|} & \frac{\mathbf{q}}{\|\mathbf{q}\|} \\ * & \frac{q_y}{\sqrt{q_x^2 + q_y^2}} & * \\ * & \frac{-q_x}{\sqrt{q_x^2 + q_y^2}} & * \\ \frac{\sqrt{q_x^2 + q_y^2}}{\sqrt{q_x^2 + q_y^2 + q_z^2}} & 0 & \frac{q_z}{\sqrt{q_x^2 + q_y^2 + q_z^2}} \end{bmatrix} \\ &= \begin{bmatrix} * & \frac{q_y}{\sqrt{q_x^2 + q_y^2}} & * \\ * & \frac{-q_x}{\sqrt{q_x^2 + q_y^2}} & * \\ \frac{\sqrt{q_x^2 + q_y^2}}{\sqrt{q_x^2 + q_y^2 + q_z^2}} & 0 & \frac{q_z}{\sqrt{q_x^2 + q_y^2 + q_z^2}} \end{bmatrix}. \end{aligned} \quad (7)$$

To recover the Euler angles from the above expression of  $R_C$ , note that if the camera is aligned with the horizontal plane, then there is no roll angle, i.e.  $\phi_C = 0$ , and  $R_C$  takes the form:

$$R_C = \begin{bmatrix} \cos(\psi_C) \cos(\theta_C) & -\sin(\psi_C) & \cos(\psi_C) \sin(\theta_C) \\ \cos(\theta_C) \sin(\psi_C) & \cos(\psi_C) & \sin(\psi_C) \sin(\theta_C) \\ -\sin(\theta_C) & 0 & \cos(\theta_C) \end{bmatrix}, \quad (8)$$

and we obtain:

$$\begin{cases} \phi_C = 0 \\ \theta_C = \text{atan2}(-\sqrt{q_x^2 + q_y^2}, q_z) \\ \psi_C = \text{atan2}(-q_y, -q_x) \end{cases} \quad (9)$$

Our cinematography system is designed to perform smooth trajectories as the UAVs are taking their shots, and then using more aggressive maneuvers only to fly between shots without filming. If UAVs fly smoothly, we can assume that their accelerations  $a_x$  and  $a_y$  are small, and hence, by direct application of Eq. (4), that their roll and pitch angles are small and  $R_x(\phi_Q) \approx R_y(\theta_Q) \approx I_3$ . This assumption is relevant to alleviate the non-linearity of the model and achieve real-time numerical optimization. Moreover, it is reasonable during shot execution, as our trajectory planner will minimize explicitly UAV accelerations, and will limit both UAV velocities and accelerations.

Under this assumption, the orientation matrix of the gimbal with respect to the quadrotor  ${}^Q_C R$  can be approximated by:

$$\begin{aligned} {}^Q_C R &= (R_Q)^T R_C \\ &\approx R_z(\psi_C - \psi_Q) R_y(\theta_C) R_x(\phi_C), \end{aligned} \quad (10)$$

and the relative Euler angles  ${}^Q_C \lambda_C$  (roll, pitch and yaw) of the gimbal with respect to the quadrotor are obtained as:

$$\begin{cases} {}^Q_C \phi_C = \phi_C = 0 \\ {}^Q_C \theta_C = \theta_C = \text{atan2}(-\sqrt{q_x^2 + q_y^2}, q_z) \\ {}^Q_C \psi_C = \psi_C - \psi_Q = \text{atan2}(-q_y, -q_x) - \text{atan2}(v_y, v_x) \end{cases} \quad (11)$$

According to Eq. (4), (9) and (11),  $\lambda_Q$ ,  $\lambda_C$  and  ${}^Q_C \lambda_C$  are completely defined by the trajectories of the quadrotor and the target, as explicit functions of  $\mathbf{q}$ ,  $\mathbf{v}_Q$ , and  $\mathbf{a}_Q$ .

### 3. Optimal Trajectory Planning

In this section, we describe our method for optimal trajectory planning. We explain how trajectories are computed online in a receding horizon scheme, considering dynamic and cinematographic constraints; and then, how the coordination between multiple UAVs is addressed. Last, we detail how to execute the trajectories and control the gimbal.

#### 3.1. Trajectory planning

We plan optimal trajectories for a team of  $n$  UAVs as they film a moving actor or target whose position can be measured and predicted. The main objective is to come up with trajectories that satisfy physical UAV and gimbal restrictions, avoid collisions and respect cinematographic concepts. This means that each UAV needs to perform the kind of motion imposed by its shot type (e.g., stay beside/behind the target in a *lateral/chase* shot) and generate smooth trajectories to minimize jerky movements of the camera and yield a pleasant video footage. Each UAV will have a shot type and a desired 3D position ( $\mathbf{p}_D$ ) and velocity ( $\mathbf{v}_D$ ) to be reached. This desired state is determined by the type of shot and may move along with the receding horizon. For instance, in a *lateral* shot, the desired position ( $\mathbf{p}_D$ ) moves with the target, to place the UAV beside it; whereas in a *flyby* shot, this position is such that the UAV gets over the target by the end of the shot. More details about the different types of shot and how to compute the desired position will be given in Section 4.

We plan trajectories for each UAV in a distributed manner, assuming that the plans from other neighboring UAVs are communicated (we denote this set of neighboring UAVs as *Neigh*). For that, we solve a constrained optimization problem for each UAV where the optimization variables are its discrete state with 3D position and velocity ( $\mathbf{x}_k = [\mathbf{p}_{Q,k} \ \mathbf{v}_{Q,k}]^T$ ), and its 3D acceleration as control input ( $\mathbf{u}_k = \mathbf{a}_{Q,k}$ ). A non-linear cost function is minimized for a horizon of  $N$  timesteps, using as input at each solving iteration the current observation of the system state  $\mathbf{x}'$ . In particular, the following non-convex optimization problem is formulated for each UAV:

$$\underset{\substack{\mathbf{x}_0, \dots, \mathbf{x}_N \\ \mathbf{u}_0, \dots, \mathbf{u}_N}}{\text{minimize}} \sum_{k=0}^N (w_1 \|\mathbf{u}_k\|^2 + w_2 J_\theta + w_3 J_\psi) + w_4 J_N \quad (12)$$

$$\text{subject to } \mathbf{x}_0 = \mathbf{x}' \quad (12.a)$$

$$\mathbf{x}_{k+1} = f(\mathbf{x}_k, \mathbf{u}_k) \quad k = 0, \dots, N-1 \quad (12.b)$$

$$\mathbf{v}_{min} \leq \mathbf{v}_{Q,k} \leq \mathbf{v}_{max} \quad (12.c)$$

$$\mathbf{u}_{min} \leq \mathbf{u}_k \leq \mathbf{u}_{max} \quad (12.d)$$

$$\mathbf{p}_{Q,k} \in \mathcal{F} \quad (12.e)$$

$$\|\mathbf{p}_{Q,k} - \mathbf{p}_{O,k}\|^2 \geq r_{col}^2, \quad \forall O \quad (12.f)$$

$$\theta_{min} \leq {}^Q_C \theta_{C,k} \leq \theta_{max} \quad (12.g)$$

$$\psi_{min} \leq {}^Q_C \psi_{C,k} \leq \psi_{max} \quad (12.h)$$

$$\cos(\beta_k^j) \leq \cos(\alpha), \quad \forall j \in \text{Neigh} \quad (12.i)$$

As constraints, we impose the initial UAV state (12.a) and the UAV dynamics (12.b), which are obtained by integrating numerically the continuous model in Section 2 with the Runge-Kutta method. We also include bounds on the UAV velocity (12.c) and acceleration (12.d), to ensure trajectory feasibility. The UAV position is restricted in two manners. On the one hand, it must stay within the volume  $\mathcal{F} \in \mathbb{R}^3$  (12.e), which is a space not necessarily convex excluding predefined no-fly zones. These are static zones provided by the director before the mission to keep the UAVs away from known hazards like buildings, high trees, crowds, etc. On the other hand, the UAV must stay at a minimum distance  $r_{col}$  from any additional obstacle  $O$  detected during flight (12.f), in order to avoid collisions.  $\mathbf{p}_{O,k}$  represents the obstacle position at timestep  $k$ . One of these constraints is added for each other UAV in the team to model them as dynamic obstacles, using their communicated trajectories to extract their positions along the planning horizon. However, other dynamic obstacles, e.g. the actor to be filmed, can also be considered. For that, a model to predict the future position of the obstacle within the time horizon is required. Besides, mechanical limitations of the gimbal to rotate around each axis are enforced by means of bounds on the pitch (12.g) and yaw angles (12.h) of the camera with respect to the UAV. Last, there are mutual visibility constraints (12.i) for each other UAV in the team, to ensure that they do not get into the field of view of the camera at hand. More details about how to compute this constraint are given in Section 3.2.

Regarding the cost function, it consists of four weighted terms to be minimized. The terminal cost  $J_N = \|\mathbf{x}_N - [\mathbf{p}_D \ \mathbf{v}_D]^T\|^2$

is added to guide the UAV to the desired state imposed by the shot type. The other three terms are related with the smoothness of the trajectory, penalizing UAV accelerations and jerky movements of the camera. Specifically, the terms  $J_\theta = |\dot{\theta}_{C,k}|^2$  and  $J_\psi = |\dot{\psi}_{C,k}|^2$  minimize the angular velocities to penalize quick changes in gimbal angles. Deriving analytically (11),  $J_\theta$  and  $J_\psi$  can be expressed in terms of the optimization variables and the target trajectory. We assume that the target position at the initial timestep is measurable and we apply a kinematic model to predict its trajectory for the time horizon  $N$ . An appropriate tuning of the different weights of the terms in the cost function is key to enforce shot definition but generating a smooth camera motion.

### 3.2. Multi-UAV coordination

Our method plans trajectories for multiple UAVs as they perform cinematography shots. The cooperation of several UAVs can be used to execute different types of shot simultaneously or to provide alternative views of the same subject. This is particularly appealing for outdoor filming, e.g. in sport events, where the director may want to orchestrate the views from multiple cameras in order to show surroundings during the line of action. In this section, we provide further insight into how we coordinate the motion of the several UAVs while filming.

The first point to highlight is that we solve our optimization problem (12) on board each UAV in a distributed manner, but being aware of constraints imposed by neighboring teammates. This is reflected in (12.f) and (12.i), where we force UAV trajectories to establish a safety distance with others and to stay out of others' field of view for aesthetic purposes. For that, we assume that UAVs are operating close to film the same scene, what allows them to communicate their computed trajectories after each planning iteration. However, there are different alternatives to synchronize the distributed optimization process so that UAVs act in a coordinate fashion. Let us discuss other approaches from key related works and then our proposal.

In the literature there are multiple works for multi-UAV optimal trajectory planning, but as we showed in Section 1.1, only few works addressed cinematography aspects specifically. A master-slave approach is applied in [5] to solve conflicts between multiple UAVs. Only one of the UAVs (the master) is supposed to be shooting the scene at a time, whereas the others act as relay slaves that provide complementary viewpoints when selected. The slave UAVs fly in formation with the master avoiding visibility issues by staying out of its field of view. Conversely, fully distributed planning is performed in [4] by means of a sequential consensus approach. Each UAV receives the current planned trajectories from all others, and computes a new collision-free trajectory taking into account the whole set of future positions from teammates and the rest of restrictions. Besides, it is ensured that trajectories for each UAV are planned sequentially and communicated after each planning iteration. In the first iteration, this is equivalent to priority planning, but not in subsequent iterations, yielding more cooperative trajectories.

We follow a hierarchical approach in between. Contrary to [5], all UAVs can film the scene simultaneously with no preferences; but there is a scheme of priorities to solve multi-UAV

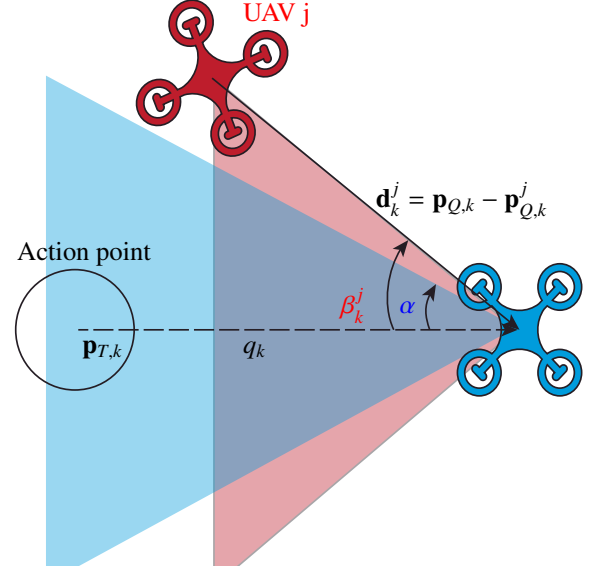


Figure 4: Mutual visibility constraint for two UAVs. The UAV on the right (blue) is filming an action point at the same time that it keeps the UAV on top (red) out of its field of view  $\alpha$ .

conflicts, as in [4]. Thus, the UAV with top priority plans its trajectory ignoring others; the second UAV generates an optimal trajectory applying collision avoidance and mutual visibility constraints given the planned trajectory from the first UAV; the third UAV avoids the two previous ones; and so on. This scheme helps coordinating UAVs without deadlocks and reduces computational cost as UAV priority increases. Moreover, we do not recompute and communicate trajectories after each control timestep as in [4]; but instead, replanning is performed at a lower frequency and, meanwhile, UAVs execute their previous trajectories as we will describe in next section.

In terms of multi-UAV coordination, constraint (12.f) copes with collisions between teammates and (12.i) with mutual visibility. We consider all neighboring UAVs as dynamic obstacles whose trajectories are known (plans are communicated), and we enforce a safety inter-UAV distance  $r_{col}$  along the entire planning horizon  $N$ . The procedure to formulate the mutual visibility constraint is illustrated in Figure 4. The objective is to ensure that each UAV's camera has not other UAVs within its angular field of view, denoted as  $\alpha$ . Geometrically, we model UAVs as points that need to stay out of the field of view, but select  $\alpha$  large enough to account for UAV dimensions. If we consider the UAV that is planning its trajectory at position  $\mathbf{p}_{Q,k}$  and another neighboring UAV  $j$  at position  $\mathbf{p}_{Q,k}^j$ , then  $\beta_k^j$  refers to the angle between vectors  $\mathbf{q}_k = \mathbf{p}_{Q,k} - \mathbf{p}_{T,k}$  and  $\mathbf{d}_k^j = \mathbf{p}_{Q,k} - \mathbf{p}_{Q,k}^j$ :

$$\cos(\beta_k^j) = \frac{\mathbf{q}_k \cdot \mathbf{d}_k^j}{\|\mathbf{q}_k\| \cdot \|\mathbf{d}_k^j\|}, \quad (13)$$

being  $\cos(\beta_k^j) \leq \cos(\alpha)$  the condition to keep UAV  $j$  out of the field of view.

Finally, it is important to notice that there may be certain situations where our priority scheme to apply mutual visibility

constraints could fail. If we plan a trajectory for the UAV with priority 1, and then, another one for the UAV with lower priority 2; ensuring that UAV 1 is not within the field of view of UAV 2 does not imply the way around, i.e., UAV 2 could still appear on UAV 1's video. However, these situations are rare in our cinematography application, as there are not many cameras pointing in random directions, but only a few and all of them filming a target typically on the ground. Moreover, since we favor smooth trajectories, we experienced in our tests that our solver tends to avoid crossings between different UAVs' trajectories, as that would result in more curves. Therefore, establishing UAV priorities in a smart way, based on their height or distance to the target, was enough to prevent issues related with mutual visibility.

### 3.3. Trajectory execution

Our trajectory planners produce optimal trajectories containing UAV positions and velocities sampled at the control timestep, which we can denote as  $\Delta t$ . As we do not recompute trajectories at each control timestep for computational reasons, we use another independent module for trajectory following, whose task is flying the UAV along its current planned trajectory. This module is executed at a rate of  $1/\Delta t$  Hz and keeps a track of the last computed trajectory, which is replaced after each planning iteration. Each trajectory follower computes 3D velocity references for the velocity controller on board the UAV. For this purpose, we take the closest point in the trajectory to the current UAV position, and then, we select another point in the trajectory at least  $L$  meters ahead. The 3D velocity reference is a vector pointing to that *look-ahead* waypoint and with the required speed to reach the point within the specified time in the planned trajectory.

At the same time that UAVs are following their trajectories, a gimbal controller is executed at a rate of  $1/\Delta t_G$  Hz to point the camera toward the target being filmed. We assume that the gimbal has an IMU and a low-level controller receiving angular rate commands, defined with respect to the world reference frame  $\{W\}$ . Using feedback about the target position, we generate references for the gimbal angles to track the target and compensate the UAV motion and possible errors in trajectory planning. These references are sent to an attitude controller that computes angular velocity commands based on the error between current and desired orientation in the form of a rotation matrix  $R_e = (R_C)^T R_C^*$ , where the desired rotation matrix  $R_C^*$  is given by (8). Recall that we assumed that  $R_C$  instantaneously takes the value of  $R_C^*$ . To design the angular velocity controller, we use a standard first-order controller for stabilization on the Special Orthogonal Group  $\mathbb{SO}(3)$ , which is given by  $\omega = k_\omega(R_e - R_e^T)^\vee$ , where the *vee* operator  $\vee$  transforms  $3 \times 3$  skew-symmetric matrices into vectors in  $\mathbb{R}^3$  [31]. More specific details about the mathematical formulation of the gimbal controller can be seen in [32].

## 4. System Architecture

In this section, we present our system architecture, describing the different software components required for trajectory

planning and their interconnection. Besides, we introduce briefly the overall architecture of our complete system for cinematography with multiple UAVs, which was presented in [33].

Our system counts on a *Ground Station* where the components related with mission design and planning are executed. We assume that there is a cinematography *director* who is in charge of describing the desired shots from a high-level perspective. We created a graphical tool and a novel cinematography language [6] to support the director through this task. Once the mission is specified, the system has planning components [7] that compute feasible plans for the mission, assigning shots to the available UAVs according to shot duration and remaining UAV flight time. The mission execution is also monitored in the Ground Station, in order to calculate new plans in case of unexpected events like UAV failures.

The components dedicated to shot execution run on board each UAV. Those components are depicted in Figure 5. Each UAV has a *Scheduler* module that receives shot assignments from the Ground Station and indicates when a new shot should be started. Then, the *Shot Executor* is in charge of planning and executing optimal trajectories to perform each shot, implementing the method described in Section 3. As input, the Shot Executor receives the future desired 3D position  $\mathbf{p}_D$  and velocity  $\mathbf{v}_D$  for the UAV, which is updated continuously by the Scheduler depending on the shot parameters and the target position. For instance, in a lateral shot, the dynamic model of the target is used to predict its position by the end of the horizon time and then place the UAV desired position at the lateral distance indicated by the shot parameters.

Additionally, the target positioning provided by the *Target Tracker* is required by the Shot Executor to point the gimbal and place the UAV adequately. In order to alleviate the effect of noisy measurements when controlling the gimbal and to provide target estimations at high frequency, the Target Tracker implements a Kalman Filter integrating all received observations. This filter is able to accept two kinds of measurements: 3D global positions coming from a GPS receiver on board the target, and 2D positions on the image obtained by a vision-based detector [8]. In particular, in the experimental setup for this paper, we used a GPS receiver on board a human target communicating measurements to the Target Tracker. Communication latency and lower GPS rates are addressed by the Kalman Filter to provide a reliable target estimation at high rate.

The Shot Executor, as it was explained in Section 3, consists of three submodules: the *Trajectory Planner*, the *Trajectory Follower* and the *Gimbal Controller*. The Trajectory Planner computes optimal trajectories for the UAV solving the problem in (12) in a receding fashion, trying to reach the desired state indicated by the Scheduler. The Trajectory Follower calculates 3D velocity commands at higher rate so that the UAV follows the optimal reference trajectory, which is updated any time the Planner generates a new solution. The Gimbal Controller generates commands for the gimbal motors in the form of angular rates in order to keep the camera pointing towards the target. The *UAV Abstraction Layer* (UAL) is a software component developed by our lab [34] to interface with the position and velocity controllers of the UAV autopilot. It provides a common

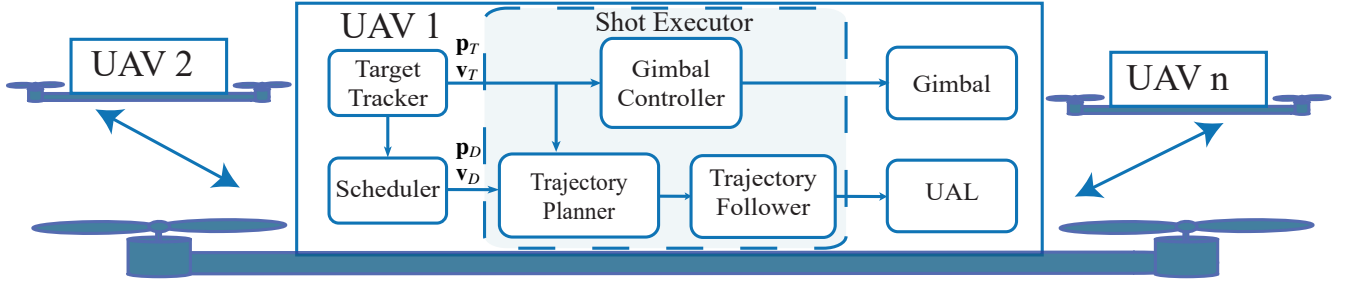


Figure 5: System architecture on board each UAV. A Scheduler initiates the shot and updates continuously the desired state for trajectory planning, whereas the Shot Executor plans optimal trajectories to perform the shot. UAVs exchange their plans for coordination.

interface abstracting the user from the protocol of each specific hardware. Finally, recall that each UAV has a communication link with other teammates in order to share their current computed trajectories, which are used for multi-UAV coordination by the Trajectory Planner.

#### 4.1. Cinematography shots

In our previous work [33], following recommendations from cinematography experts, we selected a series of canonical shot types for our autonomous multi-UAV system. Each shot has a type, a time duration and a set of geometric parameters that are used by the system to compute the desired camera position with respect to the target. The representative shots used in this work for evaluation are the following:

- *Chase/lead*: The UAV chases a target from behind or leads it in the front at a certain distance and with a constant altitude.
- *Lateral*: The UAV flies beside a target with constant distance and altitude as the camera tracks it.
- *Flyby*: The UAV flies overtaking a target with a constant altitude as the camera tracks it. The initial distance behind the target and final distance in front of it are also shot parameters.

Even though our complete system [33] implements additional shots, such as static, elevator, orbit, etc., they follow similar behaviors or are not relevant for trajectory planning evaluation. Particularly, we distinguish between two groups of shots for assessing the performance of the trajectory planner: (i) shots where the relative distance between UAV and target is constant (e.g., chase, lead or lateral), denoted as *Type I* shots; and (ii) shots where this relative distance varies throughout the shot (e.g., flyby or orbit), denoted as *Type II* shots. Note that an orbit shot can be built with two consecutive flyby shots. In Type I shots, the relative motion of the gimbal with respect to the UAV is quite limited, and the desired camera position does not vary with the shot phase, i.e., it is always at the same distance of the target. In Type II shots though, there is a significant relative motion of the gimbal with respect to the UAV, and the desired camera position depends on the shot phase, e.g., it transitions from behind to the front throughout a flyby shot. These two

$\mathbf{u}_{min}, \mathbf{u}_{max}$	$\pm 5 \text{ m/s}^2$
$\mathbf{v}_{min}, \mathbf{v}_{max}$	$\pm 1 \text{ m/s}$
$\theta_{min}, \theta_{max}$	$-\pi/2, -\pi/4 \text{ rad}$
$\psi_{min}, \psi_{max}$	$-3\pi/4, 3\pi/4 \text{ rad}$
$\alpha$	$\pi/6 \text{ rad}$
$\Delta t, \Delta t_G$	$0.1 \text{ s}$
$L$	$1 \text{ m}$

Table 1: Common values of method parameters in experiments.

kinds of patterns will result in different behaviors of our trajectory planner, so for a proper evaluation, we test it with shots from both groups.

## 5. Performance Evaluation

In this section, we present experimental results to assess the performance of our method for trajectory planning in cinematography. We evaluate the behavior of the resulting trajectories for the two categories of shots defined, demonstrating that our method achieves smooth and less jerky movements for the cameras. We also show the effect of considering physical limits for gimbal motion, as well as multi-UAV constraints due to collision avoidance and mutual visibility.

We implemented our trajectory planner described in Section 3 by means of *Forces Pro* [35], which is a software that creates domain-specific solvers in C language for non-linear optimization problems. Table 1 depicts common values for some parameters of our method used in all the experiments, where physical constraints correspond to our actual UAV prototypes. Moreover, all the experiments in this section were performed with a MATLAB-based simulation environment integrating the C libraries from Forces Pro, in a computer with an Intel Core i7 CPU @ 3.20 GHz, 8 Gb RAM.

### 5.1. Cinematographic aspects

First, we evaluate the effect of imposing cinematography constraints in UAV trajectories. For that, we selected a shot of Type II, since their relative motion between the target and the camera makes them richer to analyze cinematographic effects. Particularly, we performed a flyby shot with a single UAV, filming a target that moves on the ground with a constant velocity

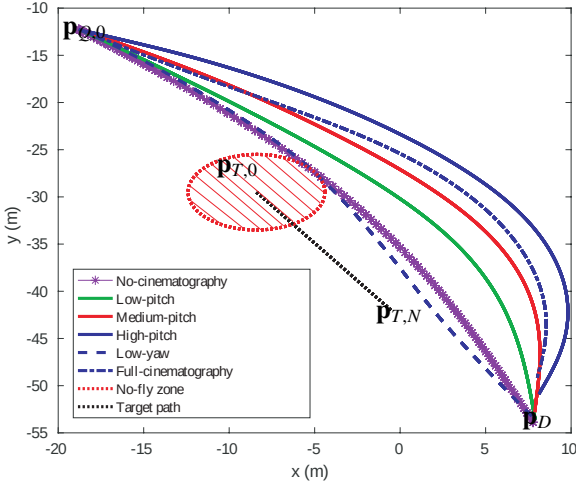


Figure 6: Top view of the resulting trajectories for different solver configurations for the cost weights. High-yaw is not shown as it was too similar to low-yaw. The target follows a straight path and the UAV has to execute a flyby shot (10 s) starting 10 m behind and ending up 10 m ahead. The predefined no-fly zone simulates the existence of a tree.

(1.5 m/s) along a straight line (this constant motion model is used to predict target movement). The UAV had to take a shot of 10 seconds at a constant altitude of 3 m, starting 10 m behind the target and overtaking it to end up 10 m ahead. Moreover, we placed a circular no-fly zone at the starting position of the target, simulating the existence of a tree.

We evaluated the quality of the trajectories computed by our method setting the horizon to  $N = 100$ , in order to calculate the whole trajectory for the shot duration (10 s) in a single step, instead of using a receding horizon<sup>2</sup>. We tested different configurations for comparison: *no-cinematography* uses  $w_2 = w_3 = 0$ ; *low-pitch*, *medium-pitch* and *high-pitch* use  $w_3 = 0$  and  $w_2 = 100$ ,  $w_2 = 1,000$  and  $w_2 = 10,000$ , respectively; *low-yaw* and *high-yaw* use  $w_2 = 0$  and  $w_3 = 0.5$  and  $w_3 = 1$ , respectively; and *full-cinematography* uses  $w_2 = 10,000$  and  $w_3 = 0.5$ . For all configurations, we set  $w_1 = w_4 = 1$ . These values were selected empirically to analyze the planner behavior under a wide spectrum of weighting options in the cost function. Figure 6 shows the trajectory followed by the target and the UAV trajectories generated with the different options. Even though trajectory planning is done in 3D, the altitude did not vary much, as the objective was to perform a shot with a constant altitude. Therefore, a top view is depicted to evaluate better the effect of the weights.

Table 2 shows a quantitative comparison of the different configurations. For this comparison, we define the following metrics. First, we measure the minimum distance to any obstacle or no-fly zone in order to check collision avoidance constraints. We also measure the *Root Mean Square Error* (RMSE) of the generated trajectory with respect to the trajectory that the UAV would follow without considering cinematographic nor colli-

<sup>2</sup>The average time to compute each trajectory was  $\sim 100$  ms, which allows for online computation.

	Dist (m)	RMSE (m)	Acc (m/s <sup>2</sup> )	Yaw jerk (rad/s <sup>3</sup> )	Pitch jerk (rad/s <sup>3</sup> )
<i>Baseline</i>	-	-	1.44	2.28	1.2
<i>No-cinematography</i>	0.00	3.97	0.86	0.61	0.31
<i>Low-pitch</i>	1.81	5.05	1.13	0.35	0.15
<i>Medium-pitch</i>	3.61	6.38	1.25	0.19	0.07
<i>High-pitch</i>	6.13	8.45	1.42	0.10	0.03
<i>Low-yaw</i>	0.00	4.19	0.81	0.52	0.25
<i>High-yaw</i>	0.00	3.51	1.00	0.50	0.23
<i>Full-cinematography</i>	4.44	7.73	1.27	0.10	0.03
<i>Full-cinematography (receding)</i>	4.19	6.87	1.45	0.08	0.03

Table 2: Resulting metrics for flyby shot. *Dist* is the minimum distance to the no-fly zone and *RMSE* the error w.r.t. the baseline trajectory. *Acc*, *Yaw jerk* and *Pitch jerk* are the average norms along the trajectory of the 3D acceleration and the jerk of the camera yaw and pitch, respectively.

sion avoidance aspects. This latter trajectory is included in Table 2 as *baseline*. For example, in the considered flyby shot, this would be the UAV overtaking the target flying on top of it, i.e., a UAV motion along the straight line that the target follows but at a higher altitude. This is the shorter way to execute the flyby, but our solver will produce different trajectories, as that option is not smooth and breaks physical constraints of the gimbal. Moreover, we measure the average norm of the 3D acceleration along the trajectory, and of the jerk (third derivative) of the camera angles  $\theta_C$  and  $\psi_C$ . These three metrics provide an idea on whether the trajectory is smooth and whether it implies jerky movement for the camera. Note that jerky motion has been identified in the literature on aerial cinematography [3, 22] as a relevant cause for low video quality.

Our experiment allows us to derive several conclusions. The *no-cinematography* configuration produces a trajectory that gets as close as possible to the no-fly zone and minimizes 3D accelerations (curved). However, when increasing the weight on the pitch rate, trajectories get further from the target and accelerations increase slightly (as longer distances need to be covered in the same shot duration), but jerk in camera angles is reduced. On the contrary, activating the weight on the yaw rate, trajectories get closer to the target and the baseline again. With the *full-cinematography* configuration, we achieve the lowest values in angle jerks and a medium value in 3D acceleration, which seems to be a pretty reasonable trade-off.

Finally, we also tested the *full-cinematography* configuration in a receding horizon manner. In that case, the solver was run at 1 Hz with a time horizon of 5 s ( $N = 50$ ). The resulting

metrics are included in Table 2. Using a receding horizon with a horizon shorter than the shot’s duration is suboptimal, and average acceleration increases slightly. However, we achieve similar values of angle jerk, plus a reduction in the computation time<sup>3</sup>. Moreover, this option of recomputing trajectories online would allow us to correct possible deviations on predictions for the target motion, in case of more random movements (in these simulations, the target moved with a constant velocity).

### 5.2. Time horizon

We also performed another experiment to evaluate the performance of shots of Type I. In particular, we selected a lateral shot to show results, but the behavior of other shots like chase or lead was similar, as they all do the same but with a different relative position w.r.t. the target. We executed a lateral shot with a duration of 20 s to film a target from a lateral distance of 8 m and a constant altitude of 3 m. As in the previous experiment, the target moves on the ground with a constant velocity (1.5 m/s) along a straight line, and we used that motion model to predict its movement. In normal circumstances, the type of trajectories followed to film the target are not so interesting, as the planner only needs to track it laterally at a constant distance. Therefore, we used this experiment to analyze the effects of modifying the time horizon, which is a critical parameters in terms of both computational load and capacity of anticipation. We used our solver in receding horizon recomputing trajectories at 2 Hz, and we placed a static no-fly zone in the middle of the UAV trajectory to check its avoidance during the lateral shot under several values of the time horizon  $N$ . The top view of the resulting trajectories (the altitude did not vary significantly) can be seen in Figure 7. Table 3 shows also the performance metrics for the different trajectories.

We can conclude that trajectories with a longer time horizon were able to predict the collision more in advance and react in a smoother manner; while shorter horizons resulted in more reactive behaviors. In general, for the kind of outdoor shots that we performed in all our experiments, we realized that time horizons in the order of several seconds (in consonance with [3]) were enough, as the dynamics of the scenes are not extremely high. We also tested that the computation time for our solver was short enough to calculate these trajectories online.

### 5.3. Multi-UAV coordination

In order to test multi-UAV coordination, we performed a new experiment combining the two types of shots from previous tests simultaneously. The target followed the same motion pattern on the ground while two UAVs filmed it during 20-second shots: one of them doing a lateral shot at 2-meter altitude and 4 m as lateral distance from the target; and the other doing a flyby shot at 4-meter altitude and starting 5 m behind the target to end up 5 m ahead. In this experiment, each UAV ran our method with a receding horizon of  $N = 80$  (8 s), recomputing trajectories at 2 Hz. We set  $r_{col} = 2$  m for collision avoidance and the low-pitch configuration for cost function weights,

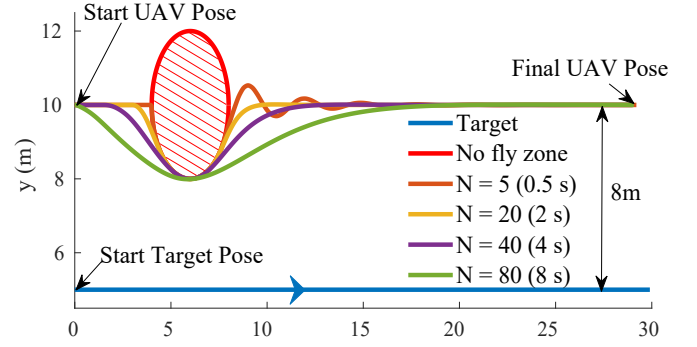


Figure 7: Receding horizon comparative for lateral shot. Top view of the resulting trajectories for different time horizons. The target follows a straight path and the UAV has to execute a lateral shot (10 s) at a 8 m distance.

Time horizon (s)	RMSE (m)	Acc ( $m/s^2$ )	Yaw jerk ( $rad/s^3$ )	Pitch jerk ( $rad/s^3$ )	Solving time (s)
0.5	1.21	0.15	10.68	1.35	0.004
2	0.9	0.08	5.12	0.32	0.016
4	1.23	0.05	5.06	0.32	0.029
8	1.3	0.04	4.8	0.29	0.101

Table 3: Resulting metrics for the lateral shot. In this case, the baseline UAV trajectory is a straight line connecting the start and final positions. *Solving time* is the average time to compute each trajectory.

as we saw this was working better for this experiment. The purpose of this experiment is to show how the trajectories are generated in such a way that both UAVs film the target without getting too close to each other or getting into each other’s field of view. Figure 4 depicts several snapshots of the simulation. Both UAVs performed their shots staying at the left side of the target motion, but it can be seen that UAV 2 modified its trajectory performing the flyby shot so that UAV 1 was never within its field of view (red cone) while filming the target laterally. For comparison, we also depict the resulting trajectories in case the UAVs did not consider each other for coordination. We established a higher priority for UAV 1 when computing trajectories, which made UAV 2 be the one affected by visibility constraints. Another option to avoid UAV 1 on the videostream of UAV 2 would be computing trajectories with changes in altitude. We preferred fixing UAVs’ altitudes for the shots, as this option produces better video footage from an aesthetic point of view.

## 6. Field Experiments

In this section, we report on field experiments to test our method with 3 UAVs filming a human actor outdoors. This allows us to verify the method feasibility with actual equipment for UAV cinematography and assess its performance in a scenario with uncertainties in target motion and detection.

<sup>3</sup>The average time to compute each trajectory was  $\sim 7ms$ .

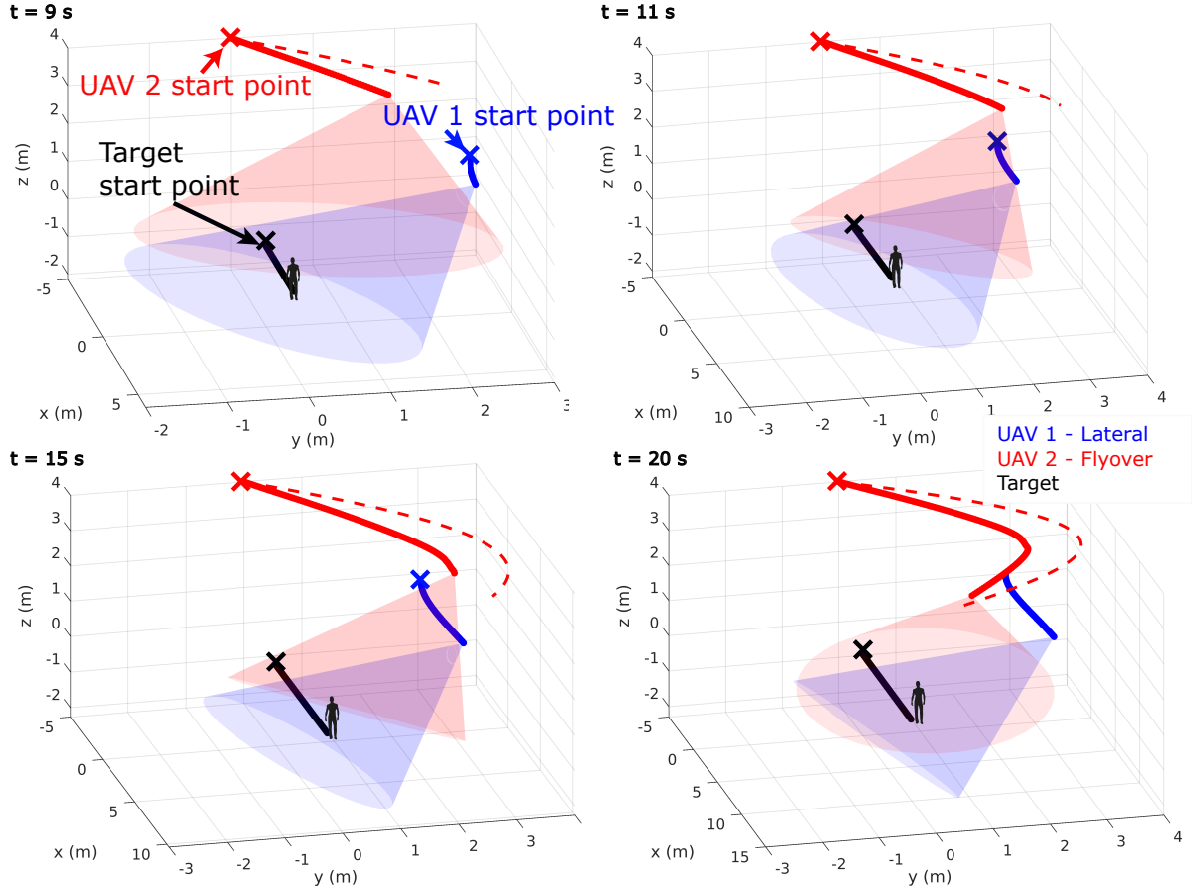


Figure 8: Different time instants of the experiment with two UAVs filming a target in a coordinated manner. UAV 1 (blue) performs a lateral shot at a 2-meter altitude and UAV 2 (red) a flyby shot at a 4-meter altitude. The trajectories generated by our method with (solid) and without (dashed) coordination are shown.

The cinematography UAVs used in our experiments were like the one in Figure 9. They were custom-designed hexacopters made of carbon fiber with a size of  $1.80 \times 1.80 \times 0.70$  m and had the following equipment: a PixHawk 2 autopilot running PX4 for flight control; a RTK-GPS for precise localization; a 3-axis gimbal controlled by a BaseCam (AlexMos) controller receiving angle rate commands; a Blackmagic Micro Cinema camera; and an Intel NUC i7 computer to run our software for shot execution. The UAVs used Wi-Fi technology to share among them their plans and communicate with our Ground Station. Moreover, as explained in Section 4, our target carried a GPS-based device during the experiments, to provide positioning measures to the Target Tracker component on board the UAVs. The device weighted around 400 grams and consisted of a RTK-GPS receiver with a Pixhawk, a radio link and a small battery. This target provided 3D measurements with a delay below 100 ms, that were filtered by the Kalman Filter on the Target Tracker to achieve centimeter accuracy. These errors were compensated by our gimbal controller to track the target on the image.

We integrated the architecture described in Section 4 into our UAVs, using the ROS framework. We developed our method for trajectory planning (Section 3) in C++<sup>4</sup>, using the frame-



Figure 9: One of the UAVs used during the field experiments.

work Forces Pro [35] to generate a compiled library for the non-linear optimization of our specific problem. The parameters used for the algorithm in the experiments were also those in Table 1. For collision avoidance, we used  $r_{col} = 5$  m, a value slightly increased for safety w.r.t. our simulations. All trajectories were computed on board the UAVs online at 0.5 Hz, with a receding horizon of  $N = 100$  (10 s). Then, the Trajectory Fol-

<sup>4</sup>[https://github.com/alfalcmr/optimal\\_navigation](https://github.com/alfalcmr/optimal_navigation).

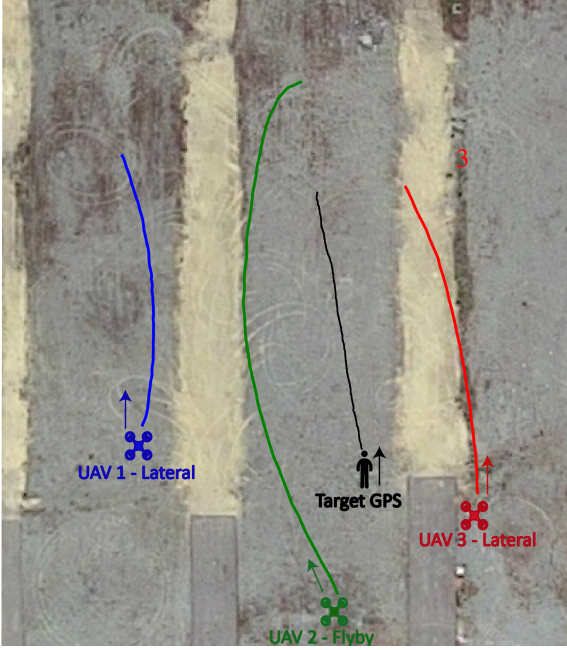


Figure 10: Trajectories followed by the UAVs and the human target during the field experiment. UAV 1 (blue) does a lateral, UAV 2 (green) a flyby and UAV 3 (red) a lateral.

lower modules generated 3D velocity commands at 10 Hz to be sent to the UAL component, which is an open-source software layer<sup>5</sup> developed by our lab to communicate with autopilot controllers. Moreover, we assumed a constant speed model for the target motion. This model was inaccurate, as the actual target speed was unknown, but those uncertainties were addressed by recomputing trajectories with the receding horizon.

We designed a field experiment with 3 UAVs taking simultaneously different shots of a human target walking on the ground. UAV 1 performs a lateral shot following the target sideways with a lateral distance of 20 m; UAV 2 performs a flyby shot starting 15 m behind the target and finishing 15 m ahead in the target motion line; and UAV 3 performs another lateral shot, but from the other side and with a lateral distance of 15 m. For safety reasons, we established different altitudes for the UAVs, 3 m, 10 m and 7 m, respectively. In our decentralized trajectory planning scheme, UAV 1 had the top priority, followed by UAV 2 and then UAV 3. Moreover, in order to design the shots of the mission safely and with good aesthetic outputs, we created a realistic simulation in Gazebo with all our components integrated and a *Software-In-The-Loop* approach for the UAVs (i.e., the actual PX4 software of the autopilots was run in the simulator).

The full video of the field experiment can be found at <https://youtu.be/M71gYva-Z6M>, and the actual trajectories followed by the UAVs are depicted in Figure 10. Figure 11 shows some example images captured by the onboard cameras during the experiment. The experiment demonstrates that our method is able to generate online trajectories for the UAVs coping with cinematographic (i.e., no jerky motion, gimbal mechanical lim-



Figure 11: Example images from the cameras on board the UAVs during the experiment: top left, UAV 1 (blue); top right, UAV 2 (green); and bottom left, UAV 3 (red). Bottom right, a general view of the experiment with the three UAVs and the target.

UAV	Traveled distance (m)	Acc (m/s <sup>2</sup> )	Dist (m)
1	95	0.125	9.543
2	141.4	0.108	9.543
3	98.6	0.100	14.711

Table 4: Metrics of the trajectories followed by the UAVs during the field experiment. We measure the total traveled distance for each UAV, the average norm of the 3D accelerations and the minimum distance (horizontally) to other UAVs.

itations and mutual visibility) and safety (i.e., inter-UAV collision avoidance) constraints; and keeping the target on the cameras' field of view, even under noisy target detections and uncertainties in its motion. Furthermore, we measured some metrics of the resulting trajectories (see Table 4) in order to evaluate the performance of our method. It can be seen that UAV accelerations were smooth in line with those produced in our simulations and the minimum distances between UAVs were always higher than the one imposed by the collision avoidance constraint (5 m).

## 7. Conclusions

In this paper, we presented a method for planning optimal trajectories with a team of UAVs in a cinematography application. We proposed a novel formulation for non-linear trajectory optimization, executed in a decentralized and online fashion. Our method integrates UAV dynamics and collision avoidance, as well as cinematographic aspects such as gimbal limits and mutual camera visibility. Our experimental results demonstrate that our method can produce coordinated multi-UAV trajectories that are smooth and reduce jerky movements. We also show that our method can be applied to different types of shots and compute trajectories online for time horizons in the order of up to 10 seconds, which seems enough for the considered cinematographic scenes outdoors. Moreover, our field experiments proved the applicability of the method with an actual team of

<sup>5</sup><https://github.com/grvcTeam/grvc-ual>.

UAV cinematographers filming outdoors.

As future work, we plan to study alternative schemes for decentralized multi-UAV coordination instead of our priority-based computation. Our objective is to compute in a distributed manner multi-UAV approximate solutions that are closer to the optimum, but without increasing significantly the computation time, and test other team approaches like a leader-followers strategy. We believe that a comparison with methods based on reinforcement learning can also be of high interest.

## References

- [1] DJI, Mavic pro 2, 2018. URL: <https://www.dji.com/es/mavic>.
- [2] Skydio, Skydio 2, 2019. URL: <https://www.skydio.com/>.
- [3] R. Bonatti, W. Wang, C. Ho, A. Ahuja, M. Gschwindt, E. Camci, E. Kayacan, S. Choudhury, S. Scherer, Autonomous aerial cinematography in unstructured environments with learned artistic decision-making, *Journal of Field Robotics* 37 (2020) 606–641. doi:10.1002/rob.21931.
- [4] T. Ngeli, L. Meier, A. Domahidi, J. Alonso-Mora, O. Hilliges, Real-time planning for automated multi-view drone cinematography, *ACM Transactions on Graphics* 36 (2017) 1–10. doi:10.1145/3072959.3073712.
- [5] Q. Galvane, C. Lino, M. Christie, J. Fleureau, F. Servant, F.-I. Tariolle, P. Guillotel, Directing cinematographic drones, *ACM Trans. Graph.* 37 (2018). doi:10.1145/3181975.
- [6] . Montes-Romero, A. Torres-Gonzlez, J. Capitn, M. Montagnuolo, S. Metta, F. Negro, A. Messina, A. Ollero, Director tools for autonomous media production with a team of drones, *Applied Sciences* 10 (2020). doi:10.3390/app10041494.
- [7] L.-E. Caraballo, . Montes-Romero, J.-M. Daz-Bnez, J. Capitn, A. Torres-Gonzlez, A. Ollero, Autonomous planning for multiple aerial cinematographers, in: *IEEE/RSJ International Conference on Intelligent Robots and Systems (IROS)*, 2020.
- [8] P. Nousi, D. Triantafyllidou, A. Tefas, I. Pitas, Joint lightweight object tracking and detection for unmanned vehicles, in: *IEEE International Conference on Image Processing (ICIP)*, 2019, pp. 160–164.
- [9] C. Richter, A. Bry, N. Roy, Polynomial Trajectory Planning for Aggressive Quadrotor Flight in Dense Indoor Environments, in: M. Inaba, P. Corke (Eds.), *International Symposium on Robotics Research (ISRR)*, Springer, 2016, pp. 649–666. doi:10.1007/978-3-319-28872-7\_37.
- [10] D. Mellinger, V. Kumar, Minimum snap trajectory generation and control for quadrotors, in: *IEEE International Conference on Robotics and Automation (ICRA)*, 2011, pp. 2520–2525. doi:10.1109/ICRA.2011.5980409.
- [11] M. Turpin, K. Mohta, N. Michael, V. Kumar, Goal assignment and trajectory planning for large teams of interchangeable robots, *Autonomous Robots* 37 (2014) 401–415. doi:10.1007/s10514-014-9412-1.
- [12] T. Baca, D. Hert, G. Loianno, M. Saska, V. Kumar, Model predictive trajectory tracking and collision avoidance for reliable outdoor deployment of unmanned aerial vehicles, in: *IEEE/RSJ International Conference on Intelligent Robots and Systems (IROS)*, 2018, pp. 1–8.
- [13] M. Kamel, J. Alonso-Mora, R. Siegwart, J. Nieto, Robust collision avoidance for multiple micro aerial vehicles using nonlinear model predictive control, in: *IEEE International Conference on Intelligent Robots and Systems (IROS)*, 2017, pp. 236–243. doi:10.1109/IR0S.2017.8202163.
- [14] E. Price, G. Lawless, R. Ludwig, I. Martinovic, H. H. Buelthoff, M. J. Black, A. Ahmad, Deep neural network-based cooperative visual tracking through multiple micro aerial vehicles, *IEEE Robotics and Automation Letters* 3 (2018) 3193–3200.
- [15] R. Tallamraju, S. Rajappa, M. J. Black, K. Karlapalem, A. Ahmad, Decentralized MPC based obstacle avoidance for multi-robot target tracking scenarios, in: *IEEE International Symposium on Safety, Security, and Rescue Robotics (SSRR)*, 2018, pp. 1–8.
- [16] V. Krtk, P. Petrček, V. Spurn, M. Saska, Autonomous reflectance transformation imaging by a team of unmanned aerial vehicles, *IEEE Robotics and Automation Letters* 5 (2020) 2302–2309.
- [17] C. Teuliere, L. Eck, E. Marchand, Chasing a moving target from a flying UAV, in: *IEEE/RSJ International Conference on Intelligent Robots and Systems (IROS)*, 2011, pp. 4929–4934. doi:10.1109/IR0S.2011.6094404.
- [18] T. Naseer, J. Sturm, D. Cremers, FollowMe: Person following and gesture recognition with a quadcopter, in: *IEEE/RSJ International Conference on Intelligent Robots and Systems (IROS)*, 2013, pp. 624–630. doi:10.1109/IR0S.2013.6696416.
- [19] M. Christie, P. Olivier, J. M. Normand, Camera control in computer graphics, *Computer Graphics Forum* 27 (2008) 2197–2218. doi:10.1111/j.1467-8659.2008.01181.x.
- [20] N. Joubert, M. Roberts, A. Truong, F. Berthouzoz, P. Hanrahan, An interactive tool for designing quadrotor camera shots, *ACM Transactions on Graphics* 34 (2015) 1–11. doi:10.1145/2816795.2818106.
- [21] N. Joubert, J. L. E. D. B. Goldman, F. Berthouzoz, M. Roberts, J. A. Landay, P. Hanrahan, Towards a Drone Cinematographer: Guiding Quadrotor Cameras using Visual Composition Principles, *ArXiv e-prints* (2016). arXiv:1610.01691.
- [22] C. Gebhardt, B. Hepp, T. Ngeli, S. Stevšić, O. Hilliges, Airways: Optimization-Based Planning of Quadrotor Trajectories according to High-Level User Goals, in: *Proceedings of the Conference on Human Factors in Computing Systems (CHI)*, 2016, pp. 2508–2519. doi:10.1145/2858036.2858353.
- [23] C. Lino, M. Christie, Intuitive and efficient camera control with the toric space, *ACM Transactions on Graphics* 34 (2015) 82:1–82:12. doi:10.1145/2766965.
- [24] Q. Galvane, J. Fleureau, F.-L. Tariolle, P. Guillotel, Automated Cinematography with Unmanned Aerial Vehicles, *Eurographics Workshop on Intelligent Cinematography and Editing* (2016). doi:10.2312/wiced.20161097.
- [25] C. Huang, F. Gao, J. Pan, Z. Yang, W. Qiu, P. Chen, X. Yang, S. Shen, K. T. Cheng, Act: An autonomous drone cinematography system for action scenes, in: *IEEE International Conference on Robotics and Automation (ICRA)*, 2018, pp. 7039–7046. doi:10.1109/ICRA.2018.8460703.
- [26] R. Bonatti, C. Ho, W. Wang, S. Choudhury, S. Scherer, Towards a robust aerial cinematography platform: Localizing and tracking moving targets in unstructured environments, in: *2019 IEEE/RSJ International Conference on Intelligent Robots and Systems (IROS)*, 2019, pp. 229–236.
- [27] T. Ngeli, J. Alonso-Mora, A. Domahidi, D. Rus, O. Hilliges, Real-time motion planning for aerial videography with dynamic obstacle avoidance and viewpoint optimization, *IEEE Robotics and Automation Letters* 2 (2017) 1696–1703. doi:10.1109/LRA.2017.2665693.
- [28] C. Huang, Z. Yang, Y. Kong, P. Chen, X. Yang, K.-T. Cheng, Learning to capture a film-look video with a camera drone, in: *IEEE International Conference on Robotics and Automation (ICRA)*, 2019, pp. 1871–1877. doi:10.1109/ICRA.2019.8793915.
- [29] M. Gschwindt, E. Camci, R. Bonatti, W. Wang, E. Kayacan, S. Scherer, Can a robot become a movie director? learning artistic principles for aerial cinematography, in: *IEEE International Conference on Intelligent Robots and Systems (IROS)*, 2019, pp. 1107–1114. doi:10.1109/IR0S40897.2019.8967592.
- [30] B. Sabetghadam, A. Alcntara, J. Capitn, R. Cunha, A. Ollero, A. Pascoal, Optimal trajectory planning for autonomous drone cinematography, in: *European Conference on Mobile Robots (ECMR)*, 2019, pp. 1–7.
- [31] T. Lee, Robust adaptive attitude tracking on SO(3) with an application to a quadrotor UAV, *IEEE Transactions on Control Systems Technology* 21 (2013) 1924–1930. doi:10.1109/TCST.2012.2209887.
- [32] R. Cunha, M. Malaca, V. Sampaio, B. Guerreiro, P. Nousi, I. Mademlis, A. Tefas, I. Pitas, Gimbal Control for Vision-based Target Tracking, in: *EUSIPCO. Satellite Workshop on Signal Processing, Computer Vision and Deep Learning for Autonomous Systems*, La Corua, Spain, 2019.
- [33] A. Alcntara, J. Capitn, A. Torres-Gonzlez, R. Cunha, A. Ollero, Autonomous execution of cinematographic shots with multiple drones, *ArXiv e-prints* (2020). arXiv:2006.12163.
- [34] F. Real, A. Torres-Gonzlez, P. R. Soria, J. Capitn, A. Ollero, Unmanned aerial vehicle abstraction layer: An abstraction layer to operate unmanned aerial vehicles, *International Journal of Advanced Robotic Systems* 17 (2020) 1–13. doi:10.1177/1729881420925011.
- [35] A. Zanelli, A. Domahidi, J. Jerez, M. Morari, FORCES NLP: an efficient implementation of interior-point methods for multistage nonlinear nonconvex programs, *International Journal of Control* (2017). doi:10.1080/00207179.2017.1316017.